How well do we understand the Planck feedback?

Timothy W. Cronin[1], **Ishir Dutta**[1]

[1]Program in Atmospheres, Ocean, and Climate, MIT, Cambridge, Massachusetts, USA

Key Points:

- Earth's reference radiative response, or "Planck feedback," is $\sim$0.5 W m^{-2} K^{-1} less stabilizing than a Stefan-Boltzmann estimate.
- We find this deviation is mostly due to the assumed lack of stratospheric warming in calculations of the Planck feedback.
- The lack of stratospheric warming serves as an implicit positive feedback in analysis of climate model warming.

Corresponding author: Timothy Cronin, twcronin@mit.edu

Abstract

A reference or "no-feedback" radiative response to warming is fundamental to understanding how much global warming will occur for a given change in greenhouse gases or solar radiation incident on the Earth. The simplest estimate of this radiative response is given by the Stefan-Boltzmann law as $-4\sigma\overline{T_e}^3 \approx -3.8$ W m^{-2} K^{-1} for Earth's present climate, where $\overline{T_e}$ is a global effective emission temperature. The comparable radiative response in climate models, widely called the "Planck feedback," averages -3.3 W m^{-2} K^{-1}. This difference of 0.5 W m^{-2} K^{-1} is large compared to the uncertainty in the net climate feedback, yet it has not been studied carefully.

We use radiative transfer models to analyze these two radiative feedbacks to warming, and find that the difference arises primarily from the lack of stratospheric warming assumed in calculations of the Planck feedback (traditionally justified by differing constraints on and time scales of stratospheric adjustment relative to surface and tropospheric warming). The Planck feedback is thus masked for wavelengths with non-negligible stratospheric opacity, and this effect implicitly acts to amplify warming in current feedback analysis of climate change. Other differences between Planck and Stefan-Boltzmann feedbacks arise from temperature-dependent gas opacities, and several artifacts of nonlinear averaging across wavelengths, heights, and different locations; these effects partly cancel but as a whole slightly destabilize the Planck feedback. Our results point to an important role played by stratospheric opacity in Earth's climate sensitivity, and clarify a long-overlooked but notable gap in our understanding of Earth's reference radiative response to warming.

Plain Language Summary

Earth's climate is stable because a warmer planet loses more energy to space, at infrared wavelengths invisible to the naked eye. The rate of change of this energy loss as the planet warms provides an estimate how Earth's energy balance responds to warming, which is simple enough to write on a small piece of paper. When scientists investigate the warming predicted by climate models, they often start from a similar but not identical calculation of how Earth's energy balance responds to warming. This calculation, based on model output, is about 15% less stabilizing than the simple pencil-and-paper estimate. In this paper, we explore the causes of this 15% difference between the pencil-and-paper estimate and the calculations using climate models. We show that the difference is primarily caused by the lack of assumed warming in climate models high in Earth's atmosphere, where temperatures are not closely linked to surface warming. This lack of warming acts as a hidden destabilizing feedback in current analysis of climate models.

1 Introduction

How much will Earth warm if atmospheric CO_2 concentrations are doubled? Answering this question with confidence draws heavily on analysis of global radiative energy balance in terms of forcings and feedbacks. Such analysis builds from a reference radiative response to warming, and is elaborated by including positive and negative feedbacks that amplify or dampen temperature change. The increase in energy radiated to space by a warmer planet provides a natural reference radiative response to warming (Hansen et al., 1984), and can be estimated using the Stefan-Boltzmann law as $-4\sigma\overline{T_e}^3 \approx -3.8$ W m^{-2} K^{-1} (e.g., Bony et al., 2006). In this calculation, we have used an effective radiating temperature $\overline{T_e} \approx 255$ K based on Earth's average outgoing longwave radiation, $\overline{\text{OLR}} \approx 240$ W m^{-2} (e.g., Loeb et al., 2018), and taking $\overline{T_e} = (\overline{\text{OLR}}/\sigma)^{1/4}$. Throughout, we will use an overline to indicate global averages, and we will refer to this blackbody estimate of Earth's reference radiative response to warming as the "Stefan-Boltzmann

feedback" ($\overline{\lambda_{SB}}$). The comparable reference radiative response calculated from comprehensive general circulation models (GCMs) – widely called the "Planck feedback" or $\overline{\lambda_P}$ (a convention we will also use) – averages only -3.3 W m^{-2} K^{-1} (Zelinka et al., 2020; Soden & Held, 2006; Bony et al., 2006, the methodology for calculating $\overline{\lambda_P}$ is described below in the introduction, and also in Sections 2 and 3). This Planck feedback value is roughly 0.5 W m^{-2} K^{-1} or 15% less stabilizing than the Stefan-Boltzmann feedback, a difference that has not been studied carefully and represents a notable foundational gap in the study of climate change in terms of forcings and feedbacks. This paper seeks to close the gap and account for the deviation between the global Planck ($\overline{\lambda_P}$) and Stefan-Boltzmann ($\overline{\lambda_{SB}} = -4\sigma\overline{T_e}^3$) feedbacks.

A difference of 15% between the Planck and Stefan-Boltzmann feedbacks might seem small, particularly since climate models agree closely on the value of the Planck feedback. The implications would be striking, however, if the Planck feedback were 0.5 W m^{-2} K^{-1} more negative and all other feedbacks remained the same. Zelinka et al. (2020) show that climate models from the coupled model intercomparison project, phases 5 and 6 (CMIP5 and CMIP6) have an average net climate feedback of -1 W m^{-2} K^{-1}. Adding -0.5 W m^{-2} K^{-1} to this would reduce total climate sensitivity by a third and would also dramatically reduce the intermodel spread in climate sensitivity. As an additional comparison point, note that the global surface albedo feedback and the global cloud feedback – both extensively studied – each have magnitude $\sim$0.5 W m^{-2} K^{-1} (Zelinka et al., 2020). It seems imprudent to allow such a large unexplained gap in Earth's reference radiative response to persist without a thorough understanding of why it arises, and upon what aspects of the climate system it depends. In practice, an alternative definition of the Planck feedback that was closer to the Stefan-Boltzmann estimate would not alter global climate sensitivity or its intermodel spread, but would result in attributing that $\sim$0.5 W m^{-2} K^{-1} to some combination of other feedbacks, altering our view of their relative importance and perhaps even altering research priorities in the study of climate change.

The conventional definition of the Planck feedback provides a major clue about the source of difference between $\overline{\lambda_P}$ and $\overline{\lambda_{SB}}$: most modern calculations of the Planck feedback neglect stratospheric temperature change. Bony et al. (2006) express the methodology succinctly:

> Note that in GCM calculations, the Planck feedback parameter is usually estimated by perturbing in each grid box the tropospheric temperature at each level by the surface temperature change predicted under climate warming. Therefore this estimate does not correspond exactly to a vertically and horizontally uniform temperature change.

This convention persists in most of the modern literature, particularly in feedback analysis that uses radiative kernels (e.g., Soden et al., 2008; Feldl & Roe, 2013; Zelinka et al., 2020). The assumption of negligible stratospheric temperature change means that one would expect the Planck feedback to be strongly masked in wavelengths where the stratosphere is optically thick, thus making the Planck feedback more positive. Below we show that "full-column" Planck feedback calculations, which include stratospheric warming, closely matche the Stefan-Bolzmann feedback (Section 2), and we find that stratospheric masking is indeed the primary reason for difference between global Planck and Stefan-Boltzmann feedbacks (Section 3).

Because the stratosphere plays a dominant role in the difference between the Planck and Stefan-Boltzmann feedbacks, a few words are warranted here about why GCM calculations neglect stratospheric warming in computing the Planck feedback. The assumption underlying this lack of stratospheric temperature change is that the stratosphere

is thermally decoupled from the surface and troposphere, and instead remains in radiative equilibrium in a perturbed climate. Furthermore, the new stratospheric radiative equilibrium state is more strongly modified by many forcing agents than it is by underlying atmospheric temperatures, and the stratosphere also responds more rapidly to perturbations than do the surface and troposphere (which are constrained by the thermal inertia of the oceans) (Hansen et al., 1997). The initial stratospheric temperature change in response to a forcing agent (such as CO_2) is thus conventionally treated as part of an "adjusted" radiative forcing, rather than as a feedback, and the combined global impact of subsequent stratospheric temperature and water vapor changes on top-of-atmosphere radiative fluxes has been found very small in past study, justifying its neglect (e.g., Huang et al., 2016). Our results in this paper do not indicate any errors in these conventional approaches, but in light of our results, we advocate for explicit recognition that the Planck feedback contains a strong destabilizing component associated with the lack of stratospheric warming. The lack of stratospheric warming acts as a large positive feedback on climate change that is hidden by current feedback analysis methods.

Our main results are simple, but considerable effort is required to dismiss other potentially relevant effects, so we have chosen a slightly unconventional structure for the paper. Section 2 is an abbreviated results section and gives a quick justification that the stratosphere is the major cause of the $\sim$0.5 W m^{-2} K^{-1} difference between Planck and Stefan-Boltzmann feedbacks. Section 3 then takes a step back to provide a more rigorous decomposition of the deviation between the local (for a single column of the atmosphere) Planck and Stefan-Boltzmann feedbacks, and to present the details of radiative transfer calculations that enable this decomposition. In addition to the dominant term of stratospheric masking, we find two other deviation terms that each have magnitude $\sim$0.1 W m^{-2} K^{-1}, but tend to cancel one another. One term, which we call "temperature-dependent opacity", is due to the general dependence of gas absorption coefficients on temperature, even at fixed concentrations, and was first discussed by Huang and Ramaswamy (2007). The other term relates to the nonlinear averaging of flux derivatives over emitting temperatures (in height) and wavenumbers (ν).

Section 4 then explores three sensitivity questions. First, does the use of a less accurate radiative transfer code matter for the deviation terms? Second, how does the deviation between Planck and Stefan-Boltzmann feedbacks depends on surface and atmospheric temperatures? Third, does the stratospheric masking term always need to dominate the difference between local Planck and Stefan-Boltzmann feedbacks, or can the minor terms contribute much more under very different atmospheric compositions?

Section 5 assesses artifacts of global averaging and is not essential to the flow of the paper. Global-mean Planck and Stefan-Boltzmann feedbacks are not obtained from their local values by identical averaging processes. We find that differences in spatial and temporal averaging are generally a minor effect, but do tend to make the Planck feedback slightly less negative due to spatiotemporal covariance between local Planck feedback values and the global warming pattern: it tends to warm most where it is cold and the Planck feedback is least negative.

Finally, section 6 closes with a discussion of limitations of this work, relation to past work, and future directions. We reiterate our perspective that there is no active error in current conventions surrounding the Planck feedback; nevertheless, a large positive feedback associated with the lack of stratospheric warming is hiding in plain sight, and deserves more attention in future work.

2 The dominant role of the stratosphere

Our primary question is this: why is the Planck feedback, calculated following GCM conventions, $\sim$0.5 W m^{-2} K^{-1} more positive than the Stefan-Boltzmann feedback? For

a single column of the atmosphere, the local Planck feedback is given by an integral over wavenumber ν of the top-of-atmosphere flux change δF_0^ν (where the subscript $_0$ indicates the top-of-atmosphere, and the superscript $^\nu$ indicates that the flux depends on wavenumber) per unit vertically uniform warming of the surface and troposphere, denoted δT_T:

$$\lambda_P = -\int_0^\infty \frac{\delta F_0^\nu}{\delta T_T} d\nu, \tag{1}$$

whereas the local Stefan-Boltzmann feedback is calculated as the derivative of the blackbody flux with respect to temperature ($\pi dB^\nu/dT$, where B^ν is the Planck function), evaluated at the effective emission temperature (T_e):

$$\lambda_{SB} = -\int_0^\infty \pi \frac{dB^\nu(T_e)}{dT} d\nu = -4\sigma T_e^3 = 4\sigma^{1/4}\mathrm{OLR}^{3/4}. \tag{2}$$

A line-by-line radiative transfer model, LBLRTM (Clough et al., 2005), is used to calculate λ_P and λ_{SB} for an reference idealized atmospheric profile, with surface air temperature of 290 K. Details of the calculations, including thermal structure and trace gases used, are provided below (Section 3.2). For the sake of brevity, we skip directly to the results.

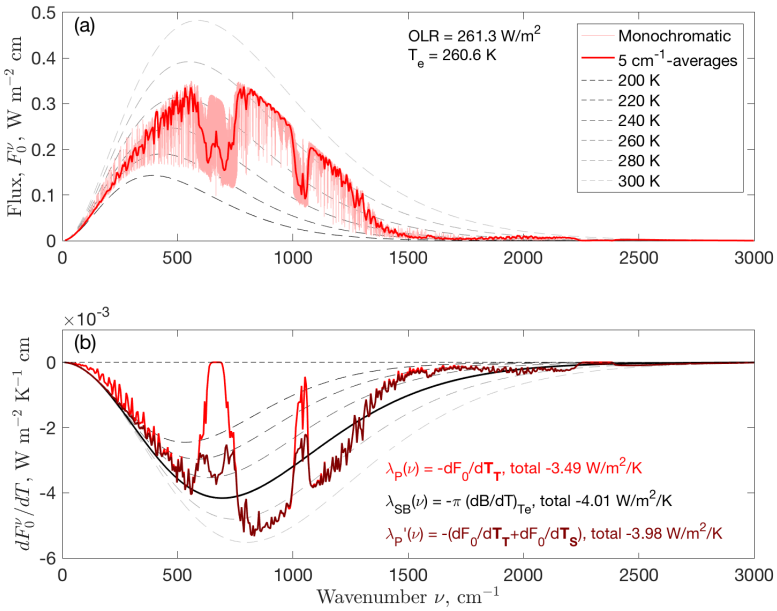

Figure 1. a) Outgoing infrared flux spectrum with the line-by-line radiative transfer model LBLRTM, for a clear-sky atmosphere with a surface temperature of 290 K, with monochromatic irradiances shown in pink, and 5 cm^{-1}-band averages in red. Thin dashed lines from black to light gray indicate reference blackbody spectra. b) Spectrally-resolved Planck feedback ($\lambda_P(\nu)$, red), Stefan-Boltzmann feedback ($\lambda_{SB}(\nu)$, black), and "full column" Planck feedback ($\lambda'_P(\nu)$, dark red).

Our reference atmosphere has OLR=261.3 W m^{-2} (~5-10 W m^{-2} smaller than the observed clear-sky global-mean, e.g., Loeb et al., 2018), an effective emission temperature $T_e = (\mathrm{OLR}/\sigma)^{1/4} = 260.6$ K, and thus a local Stefan-Boltzmann feedback of -4.01 W m^{-2} K^{-1} (Figure 1). A calculation with the surface and troposphere cooled by 1K

(cooling rather than warming is used due to the set of numerical experiments described in Appendix A), however, shows that the Planck feedback is less negative than λ_{SB} by 0.52 W m^{-2} K^{-1}: $\lambda_P = -3.49$ W m^{-2} K^{-1} (red curve in Figure 1b). This is similar to the global clear-sky temperature feedback of -3.56 W m^{-2} K^{-1} found by Soden et al. (2008). An important role for the stratosphere can be inferred from the lack of flux change with warming in the center of the CO_2 band around 660 cm^{-1}, where the stratosphere is most opaque (Figure 1b). This role is confirmed by calculating a "full-column" Planck feedback λ'_P, which cools the entire column including the stratosphere by 1K (denoting vertically uniform warming of the stratosphere as δT_S):

$$\lambda'_P = -\int_0^\infty \left(\frac{\delta F_0^\nu}{\delta T_T} + \frac{\delta F_0^\nu}{\delta T_S} \right) d\nu. \tag{3}$$

With $\lambda'_P = -3.98$ W m^{-2} K^{-1}, this "full-column" Planck feedback is only 0.03 W m^{-2} K^{-1} larger than λ_{SB} (dark red curve in Figure 1b). Including stratospheric warming thus gives the missing ∼0.5 W m^{-2} K^{-1} increase in OLR with warming that we sought: these calculations indicate that the lack of stratospheric warming in the conventional Planck feedback is the dominant reason for the difference between local Planck and Stefan-Boltzmann feedbacks.

Fully closing the gap between λ_P and λ_{SB} requires a more careful decomposition, developed below, which reveals some additional effects that contribute but tend to cancel one another (Section 3). A reader interested only in the role of the stratosphere, and the implications of the findings shown above, may wish to skip directly to the conclusions section (Section 6).

3 Local deviation terms

3.1 Definitions

The "full-column" Planck feedback (λ'_P) and Stefan-Boltzmann feedback (λ_{SB}) in Figure 1b agree quite closely when integrated over the spectrum, but do not match one another at individual wavenumbers. This motivates us to exactly decompose the difference between the local Planck feedback and Stefan-Boltzmann feedback as a sum of deviation terms. The three resulting deviation terms, when integrated across wavenumbers, correspond to one dominant term of stratospheric masking (matching our findings above in Figure 1), and two smaller terms: temperature-dependent opacity and nonlinear averaging.

We start by noting that the flux changes $\frac{\delta F_0^\nu}{\delta T_T}$ in Equation 1 can be further decomposed into one part from increases in Planck source function with warming $(\delta F_0^\nu)_{\text{Planck}}$, and another associated with changes in gas optical properties, $(\delta F_0^\nu)_{\text{optics}}$:

$$\lambda_P = -\int_0^\infty \left[\left(\frac{\delta F_0^\nu}{\delta T_T} \right)_{\text{Planck}} + \left(\frac{\delta F_0^\nu}{\delta T_T} \right)_{\text{optics}} \right] d\nu. \tag{4}$$

Adding and subtracting λ_{SB} from the right-hand side (with spectrally-resolved form $-\pi dB^\nu(T_e)/dT$ as in Equation 2), adding and subtracting the flux derivative per unit stratospheric temperature change due to the stratospheric Planck source, $(\delta F_0^\nu/\delta T_S)_{\text{Planck}}$ (where δT_S denotes only stratospheric warming), and regrouping terms, gives:

$$\begin{aligned} \lambda_P = \lambda_{SB} \quad & \underbrace{+\int_0^\infty \left(\frac{\delta F_0^\nu}{\delta T_S} \right)_{\text{Planck}} d\nu}_{\Delta_S} \underbrace{-\int_0^\infty \left(\frac{\delta F_0^\nu}{\delta T_T} \right)_{\text{optics}} d\nu}_{\Delta_T} \\ & \underbrace{-\int_0^\infty \left[\left(\frac{\delta F_0^\nu}{\delta T_T} \right)_{\text{Planck}} + \left(\frac{\delta F_0^\nu}{\delta T_S} \right)_{\text{Planck}} - \pi \frac{dB^\nu(T_e)}{dT} \right] d\nu}_{\Delta_N}. \end{aligned} \tag{5}$$

In equation 5, each underbrace defines a deviation term:

$$\begin{aligned} \lambda_P &= \lambda_{SB} + \Delta_S + \Delta_T + \Delta_N \\ \Delta_S &: \text{stratospheric masking} \\ \Delta_T &: \text{temperature} - \text{dependent opacity} \\ \Delta_N &: \text{nonlinear averaging.} \end{aligned} \tag{6}$$

The stratospheric masking deviation, Δ_S, is the derivative of the top-of-atmosphere flux with respect to stratospheric temperature due to the changes in the stratosphere's Planck source function – as discussed above, this term is "missing" from the standard definition of λ_P because stratospheric temperatures are conventionally held constant. The phrase "missing stratospheric emission" would thus also be a good descriptor for Δ_S, and is in some ways more precise as it highlights that both the stratospheric opacity and thermal structure play a role in its value; we have opted against using it because it is a longer phrase, and less intuitive for some. It should be noted that "missing stratospheric emission" and "stratospheric masking" are inseparable complementary effects. In wavelengths with appreciable stratospheric opacity, changes in upwelling flux at the tropopause are attenuated at the top of the atmosphere regardless of stratospheric temperature change, and the lack of assumed stratospheric warming means that there is no contribution from the stratosphere itself to a change in top-of-atmosphere flux.

The temperature-dependent opacity term, Δ_T, is not included in the Stefan-Boltzmann feedback and represents physics of gas absorption coefficients that strengthen or weaken with warming. This effect is entirely distinct from the variation of blackbody radiation with temperature. The nonlinear averaging deviation, Δ_N, is the difference between the whole-column changes in Planck source function with warming and the derivative of blackbody emission with respect to temperature, evaluated at T_e. The nonlinear averaging deviation includes contributions both from nonlinear averaging over heights at a given wavenumber and nonlinear averaging across wavenumbers; in Appendix B we show that the former term is usually small.

Because the "full-column" Planck feedback, λ'_P, includes contributions from both Planck source term and gas optics for both troposphere and stratosphere (Equation 3), it can be written as follows:

$$\lambda'_P = \lambda_{SB} + \Delta_N + \Delta_T - \int_0^\infty \left(\frac{\delta F_0^\nu}{\delta T_S} \right)_{\text{optics}} d\nu. \tag{7}$$

We thus expect λ'_P to be close to λ_{SB} only if Δ_N, Δ_T, and a stratospheric temperature-dependent opacity term all sum together to a small value when integrated over the spectrum.

3.2 Radiative transfer calculations

Calculations are performed with the line-by-line radiative transfer model LBLRTM (Clough et al., 2005), version 12.2, using the MT_CKD2.5 continuum, and AER version 3.2 line files, based on HITRAN2008 data. We use a spectral resolution of $\delta\nu \sim 0.01$ cm^{-1} over the thermal infrared from $\nu = 10 - 3500$ cm^{-1}, so a few hundred thousand monochromatic radiative transfer calculations are done for each profile. This allows for the effects of individual lines (typically with widths $\sim$0.1 cm^{-1} at sea-level pressure) to be resolved. Output is also averaged over 5 cm^{-1} bands for plotting.

Our reference idealized atmospheric profile has a surface temperature $T_g = 290$ K, a moist pseudoadiabatic troposphere with 80% relative humidity, and a stratosphere with a constant lapse rate $dT/dz = 1.8$ K km^{-1} above the height where temperatures fall to a specified tropopause temperature of 200 K (for this profile, 12.5 km). The surface pressure is set to 1000 hPa, and the 1000-hPa air temperature equals the surface

temperature. The specific humidity in the stratosphere is set to a uniform 5 ppmv (similar to observed mid-stratospheric values; e.g., Oman et al., 2008), and the ozone profile follows the gamma distribution in pressure from Wing et al. (2018). The reference profile includes 400 ppmv of CO_2, and no other well-mixed greenhouse gases. These choices represent a compromise between a profile reasonably close to global-average conditions, while also being simple and easily generalized to different surface temperatures. The dry atmosphere is taken to be 79% N_2 and 21% O_2 (relevant for pressure-broadening of lines). The vertical grid spacing is 500 m, fluxes are integrated to a height of 50 km, and gas absorber amounts are scaled by a factor of 5/3 to account for the slant path taken by thermal radiation through the atmosphere (Elsasser, 1942).

We perform only clear-sky calculations to assess the local deviation terms, and this choice merits a brief explanation. Because clouds reduce OLR and mask the flux changes from warmer underlying layers, they will reduce the values of both the Stefan-Boltzmann and Planck feedbacks (e.g., Soden et al., 2008) – but this paper is focused on the differences between the two. By construction, tropospheric clouds will have no effect whatsoever on Δ_S, as stratospheric masking depends only on stratospheric opacity and temperature structure. By reducing the outgoing flux and smoothing its spectrum towards that of a blackbody at cloud-top temperature, optically thick cloud layers – especially in the upper troposphere – would likely reduce the magnitudes of both Δ_T and Δ_N. Our central findings of stratospheric masking being most important, and temperature-dependent opacity and nonlinear averaging nearly cancelling one another, thus should be largely insensitive to clouds.

The set of numerical calculations used to compute the flux derivatives and isolate the contributions of the different terms in Equations 5 and 6 is somewhat technical, and is thus described in Appendix A.

3.3 Results

We revisit our Planck feedback calculation from Figure 1, but with the deviation terms now enabling an exact decomposition of the difference between Planck and Stefan-Boltzmann feedbacks (Figure 2). In this figure, it now exactly holds at each wavenumber that $\lambda_P(\nu) = \lambda_{SB}(\nu) + \Delta_S(\nu) + \Delta_T(\nu) + \Delta_N(\nu)$, or that the red line equals the black line plus the blue, gold, and purple lines.

The stratospheric masking deviation, $\Delta_S(\nu) = (\delta F_0^\nu / \delta T_S)_{\text{Planck}}$ (Figure 2a, blue), acts as a positive feedback in the parts of the spectrum where the stratosphere is optically thickest: the CO_2 band (near 660 cm^{-1}), the O_3 band (near 1000 cm^{-1}), and the strongest lines of the water vapor rotational band (wavenumbers less than 500 cm^{-1}). As suggested by Figure 1, Δ_S accounts almost entirely for the spectrally-integrated difference of 0.52 W m^{-2} K^{-1} between λ_P and λ_{SB} . The temperature-dependent opacity deviation $\Delta_T(\nu) = -(\delta F_0^\nu / \delta T_T)_{\text{optics}}$ (Figure 2a, gold), integrates across wavenumbers to a small positive feedback of 0.07 W m^{-2} K^{-1}, with positive contributions on the flanks of the CO_2 and water vapor bands outweighing negative contributions within the atmospheric window region (particularly from 800-1000 cm^{-1}), where continuum absorption by H_2O dominates over line absorption. The edges of CO_2 and H_2O bands have line strengths that depend particularly strongly on temperature because their lower-level states have high rotational quantum numbers and thus high lower-level energies, so molecular populations in the absorbing lower-level quantum state increase rapidly with warming. Continuum absorption, on the other hand, decreases with temperature if gas partial pressures are held fixed with warming. The spectral features of our temperature-dependent opacity deviation term compare closely to the "absorptivity effect" first discussed by Huang and Ramaswamy (2007) (see their Figure 4), though we find a smaller magnitude of Δ_T (likely in part because Huang and Ramaswamy (2007) also include stratospheric warming). The nonlinear averaging deviation, $\Delta_N(\nu)$ (Figure 2a, purple), varies in sign across

the spectrum, tracking the difference between the monochromatic brightness temperature (T_b^ν) and the effective emission temperature T_e. Δ_N integrates to a small negative feedback of -0.06 W m^{-2} K^{-1} and thus almost cancels Δ_T.

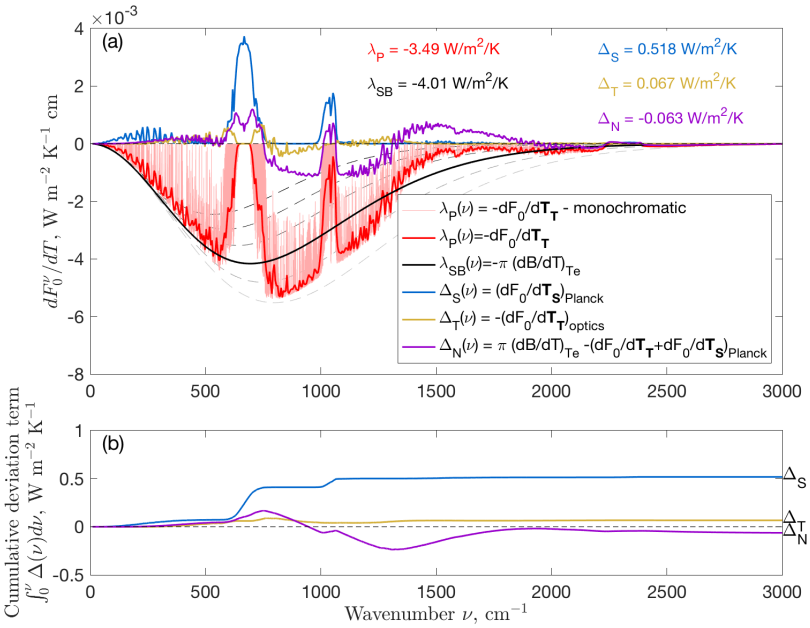

Figure 2. a) Spectrally-resolved Planck feedback ($\lambda_P\nu$, monochromatic in pink, 5 cm^{-1}-band averages in red), Stefan-Boltzmann feedback ($\lambda_{SB}(\nu)$, black), and the spectrally-resolved deviation terms Δ_S (blue), Δ_T (gold), and Δ_N (purple). Thin dashed lines from black to light gray show negative values of the derivative of the Planck function for the same reference temperatures as in Figure 1a. b) Cumulative integrals from 0 to wavenumber ν of each deviation term. The value at the right-hand side of the plot indicates the full spectral integral of the deviation term Δ, and wavenumbers of greatest slope indicate areas most important to the term.

Cumulative integrals of each deviation term in wavenumber (Figure 2b) provide another way of showing what spectral regions contribute most to each term. The stratospheric masking term derives about ~60% of its value from the CO_2 band, and about ~20% each from H_2O and O_3 bands (Figure 2b, blue). The temperature-dependent opacity term, Δ_T, derives about half of its value from CO_2 bands and half from H_2O bands (Figure 2b, gold). Finally, the nonlinear averaging term, Δ_N, has a large magnitude across the spectrum, since most wavenumbers do not have T_b^ν close to T_e. The cumulative integral of Δ_N shows that negative contributions in the atmospheric window region from 800-1300 cm^{-1}, where $T_b^\nu > T_e$, outweigh positive contributions in strongly absorbing bands of CO_2, H_2O, and O_3, where $T_b^\nu < T_e$ (Figure 2c, purple). The positive contributions to Δ_N by strongly absorbing bands are not proportional to the greenhouse effect of each band, or the amount by which it reduces OLR. For example, the combination of the H_2O rotational and CO_2 rotational-vibrational bands (~0-750 cm^{-1}) contribute about 0.2 W m^{-2} K^{-1} to Δ_N, which is similar to the impact of the H_2O rotational-vibrational band (~1250-2000 cm^{-1}), but the two former bands have a much larger greenhouse effect than the latter one. This mismatch occurs because the high-wavenumber tail of the Planck function accounts for a much larger share of $dB^\nu(T)/dT$ as compared to $B^\nu(T)$, so absorbers at high wavenumbers matter more in a relative sense for the Planck feedback than they do for OLR.

4 Sensitivity tests

4.1 Sensitivity to model: calculations with RRTMG

We first examine how the results above may depend use of a simpler radiative transfer scheme. For computational efficiency, climate models typically use radiation parameterizations that approximately solve atmospheric radiative transfer equations at many fewer wavenumbers than in a line-by-line calculation. For example, RRTMG (the Rapid Radiative Transfer Model for GCMs, Clough et al., 2005) – a widely used scheme in climate models – uses the correlated-k approximation, in which the thermal spectrum is first broken up into bands (16 bands for RRTMG from 10-3250 cm^{-1}; for example, one strong CO_2 band spans 630-700 cm^{-1}). A small number of full radiative transfer calculations are then performed by grouping wavenumbers in each band with similar gas absorption coefficients (called g-points). Thus, in RRTMG, only 140 radiative transfer calculations are done for each profile, and the temperature-dependence of absorption coefficients is implemented by lookup tables rather than by explicit calculations of line strengths. The benchmark accuracy of RRTMG relative to LBLRTM is $\sim$1 W m^{-2} for net longwave fluxes at any altitude (Clough et al., 2005). To test whether the approximations in RRTMG matter for the deviation terms, we have repeated the above calculations but using RRTMG rather than LBLRTM.

For the reference atmospheric profile, agreement between the two models is good but not perfect. The OLR and Stefan-Boltzmann feedback in RRTMG compare quite closely (within 1%) with the calculations from LBLRTM, and each deviation term in RRTMG also matches the sign and relative magnitude of that found in LBLRTM (Figure 3). The Planck feedback from RRTMG, however, is more negative than that calculated with LBLRTM by 0.13 W m^{-2} K^{-1}, with Δ_S and Δ_N both being slightly lower in RRTMG than in LBLRTM. The discrepancy is small for the nonlinear averaging term, and the use of band-averaged data in RRTMG limits our ability to explore it further. The stratospheric masking term seems smaller in RRTMG than in LBLRTM because the emissivity of the stratosphere in the O_3 band and the wings of the CO_2 band is underestimated by RRTMG. Such underestimation of stratospheric opacity, particularly in the O_3 band, is a documented error of the correlated-k approximation, likely associated with "blurring," whereby the sorting of wavenumbers by absorption coefficient is imperfectly correlated at different heights in the atmosphere (Fu & Liou, 1992).

Overall, the results of these calculations suggest that the radiative transfer code used in many GCMs is sufficient to capture the physics and general size of the deviation terms discussed above, but that stratospheric opacity may be underestimated in GCMs that use RRTMG or other radiative transfer schemes with the correlated-k approximation.

4.2 Sensitivity to surface temperature

Is the latitudinal variation of λ_P mostly captured by variations in T_e, or do the deviation terms also vary systematically with surface temperature? With fixed tropopause temperature, we expect higher surface temperatures to mean a lower tropopause pressure, a less massive and optically thinner stratosphere, and thus smaller values of Δ_S. It is less clear how the other two deviation terms might vary with surface temperature. To explore these questions, we use calculations with atmospheres over surface temperatures (T_g) ranging from 260-310 K, using both LBLRTM and RRTMG. Temperature profiles again follow a moist adiabat in the troposphere up to a tropopause temperature of 200 K, and temperatures increase with height at 1.8 K km^{-1} in the stratosphere. Tropospheric relative humidity, stratospheric specific humidity, CO_2, and O_3 profiles are all identical to the reference calculation.

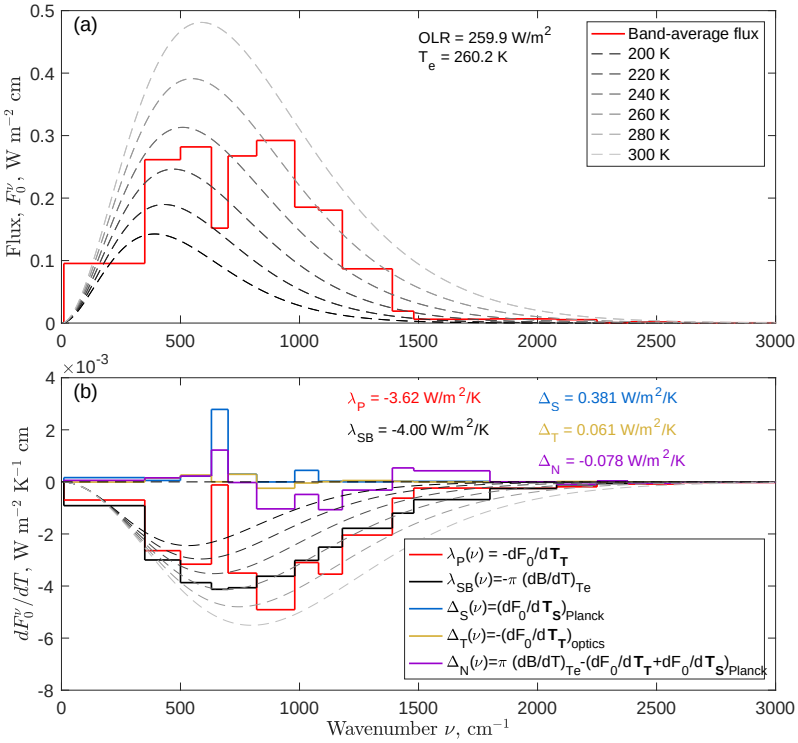

Figure 3. a) Outgoing infrared flux spectrum with the correlated-k radiative transfer model RRTMG, for the same atmospheric temperature and trace-gas profiles as used in Figures 1 and 2. Thin dashed lines from black to light gray show reference blackbody spectra. b) Band-averaged Planck feedback ($\lambda_P\nu$, red), Stefan-Boltzmann feedback ($\lambda_{SB}(\nu)$, black), and deviation terms Δ_S (blue), Δ_T (gold), and Δ_N (purple). Thin dashed lines from black to light gray show negative values of the derivative of the Planck function for the same reference temperatures as in a). Total values of each deviation term are included in b).

The Planck feedback varies more with surface temperature than does the Stefan-Boltzmann feedback, with λ_P becoming closer to λ_{SB} at high surface temperatures (Figure 4a). This greater sensitivity to temperature indicates that the sum of the deviation terms $\Delta_S + \Delta_T + \Delta_N$ becomes less positive with surface warming, and arises mainly from stratospheric masking and temperature-dependent opacity terms; nonlinear averaging varies comparatively little with surface temperature (Figure 4b). As the surface warms at constant tropopause temperature, the stratosphere thins, stratospheric opacity decreases, and Δ_S decreases. Across all surface temperatures Δ_S is smaller for RRTMG than for LBLRTM (as discussed above), but the sensitivity to surface temperature is similar in both models. The temperature-dependence of Δ_T occurs due to the competition between the H_2O continuum, which decreases in optical thickness with warming, and other absorption bands, which mostly increase in optical thickness with warming. Continuum absorption becomes important only for $T_g \geq 290$K, and its increasing role switches the sign of Δ_T from positive to negative as the surface warms. Specifically, the continuum region from 800-1300 cm^{-1} contributes about 0.01 W m^{-2} K^{-1} to Δ_T for surface temperatures of 260-280 K, -0.03 W m^{-2} K^{-1} for $T_g = 290$ K, -0.13 W m^{-2} K^{-1} for $T_g = 300$ K, and -0.2 W m^{-2} K^{-1} for $T_g = 310$ K. Differences in Δ_T between LBLRTM and RRTMG seen at both the warmest and coldest surface temperatures could be associated with extrapolation of RRTMG absorption coefficients outside the temperature ranges

of the lookup table: Kluft et al. (2021) found this will occur in the upper troposphere for moist adiabats originating from surface temperatures colder than 280 K or warmer than 306 K.

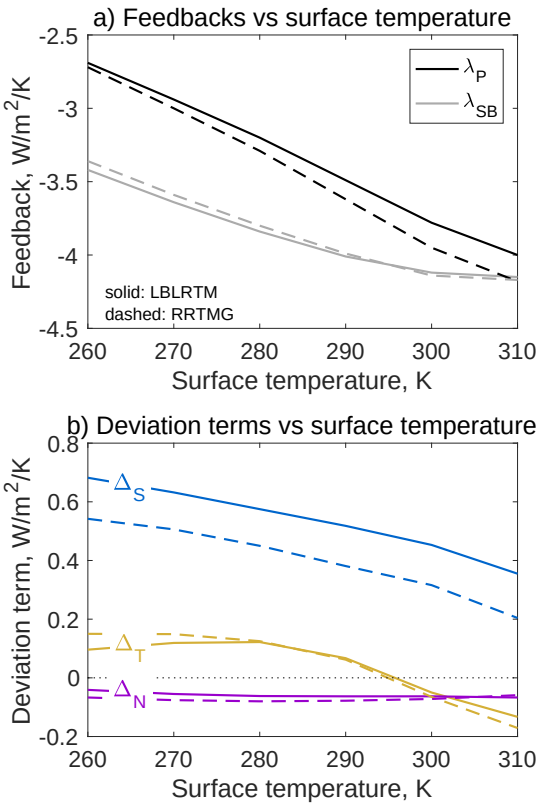

Figure 4. a) Planck λ_P and Stefan-Boltzmann λ_{SB} feedbacks over a range of surface temperatures, for calculations with LBLRTM (solid) and RRTMG (dashed). b) Spectrally integrated deviation terms for stratospheric masking (Δ_S), temperature-dependent opacity (Δ_T), and nonlinear averaging (Δ_N) over a range of surface temperatures, for calculations with LBLRTM (solid) and RRTMG (dashed).

Using the $T_g = 260$ K and $T_g = 300$ K calculations from LBLRTM as representative of the pole-equator temperature difference on Earth, the difference between λ_{SB} values at these two surface temperatures is 0.7 W m^{-2} K^{-1}, whereas the difference in λ_P is 1.09 W m^{-2} K^{-1}. These results indicate that the deviation terms increase $|d\lambda_P/dT_g|$ by over 50% as compared to $|d\lambda_{SB}/dT_g|$. In LBLRTM, stratospheric masking accounts for about 60% of this greater sensitivity of the Planck feedback to surface temperature, temperature-dependent opacity accounts for 35%, and nonlinear averaging the remaining 5%. Calculations with RRTMG also show that $|d\lambda_P/dT_g|$ exceeds $|d\lambda_{SB}/dT_g|$, with the parameterized temperature-dependent opacity accounting for a larger fraction of the effect in that model. To our knowledge, this systematic dependence of the Planck feedback on surface temperature, through factors not linked to T_e, is a previously unrecognized facet of climate feedback analysis.

4.3 Sensitivity to atmospheric composition

To give an illustration of how temperature-dependent opacity and nonlinear averaging terms need not remain small or cancel one another, we examine the Planck feedback for a dramatically different atmospheric composition, while holding the local Stefan-Boltzmann feedback constant. We modify the reference case by removing all atmospheric H_2O, while greatly increasing CO_2 to obtain the same OLR=261.3 W m^{-2} as the reference case. The modified atmosphere has 19.5% CO_2, no O_3, a dry-adiabatic lapse rate in the troposphere, and an isothermal stratosphere at a temperature of 200 K. These choices give a markedly different OLR spectrum: at wavenumbers of 200-500 cm^{-1}, emission looks nearly like that of a blackbody, but at higher wavenumbers, several CO_2 bands (from about 550-800, near 950, 1100, 1250, and 1350 cm^{-1}) cut deeply into the outgoing flux spectrum (Figure 5a). This profile has the same value of $\lambda_{SB} = -4.01$ W m^{-2} K^{-1}, but now $\lambda_P = -2.99$ W m^{-2} K^{-1}, a further 0.5 W m^{-2} K^{-1} less negative than the reference case. Stratospheric masking remains the largest deviation term, with a value of 0.54 W m^{-2} K^{-1} (slightly larger than the reference case). Temperature-dependent opacity and nonlinear averaging deviations, however, differ much more relative to our calculations above: $\Delta_T = 0.39$ W m^{-2} K^{-1} is larger by nearly a factor of six, and $\Delta_N = 0.09$ W m^{-2} K^{-1} has changed signs and increased somewhat in magnitude. The stratospheric masking term is still large because the increased abundance of CO_2 makes the stratosphere optically thick across more of the spectrum, compensating for a smaller Planck source from a cooler stratosphere and lack of stratospheric opacity in H_2O and O_3 bands. The temperature-dependent opacity term is large because the flanks of the CO_2 bands (near 550, 800, 950, and 1100 cm^{-1} in Figure 5) have line strengths that are particularly sensitive to temperature, and because there is no cancelling contribution from weakening H_2O continuum absorption with warming. Finally, the nonlinear averaging term has changed signs because the primary "atmospheric window" where $T_b^\nu > T_e$ now lies at low wavenumbers where the value of dB^ν/dT is smallest relative to B^ν, and higher wavenumbers are more evenly split between brightness temperatures above and below T_e.

This example indicates that difference between the Planck and Stefan-Boltzmann feedbacks could be much larger, and that the cancellation between Δ_T and Δ_N found in the present climate need not hold for different atmospheric compositions. The deviation terms Δ_T and Δ_N in this example could be viewed as important positive feedbacks of their own, with their sum being comparable in magnitude to the surface albedo or cloud feedbacks in current climate models (e.g., Zelinka et al., 2020). This specific example also suggests that worlds with dry, CO_2-rich atmospheres could show greater climate sensitivities than we would anticipate from the Stefan-Boltzmann feedback.

5 Global averaging

We have thus far focused only on local values of the Planck and Stefan-Boltzmann feedbacks. In this section, we address the issue that global averaging methods for the two feedbacks are not the same, which could lead to differences between their global-mean values even if their local values were identical. Specifically, we show that only a ∼0.1 W m^{-2} K^{-1} discrepancy between $\overline{\lambda_P}$ and $\overline{\lambda_{SB}}$ can be explained by artifacts of global averaging, leaving the bulk of the difference to be explained by (previously documented) local deviation terms.

Averaging methods differ because the global-mean Planck feedback, $\overline{\lambda_P}$, is a weighted average of local feedbacks based on local temperature changes (in latitude, longitude, and time), so any covariance between the warming pattern and local Planck feedback will cause $\overline{\lambda_P}$ to differ from a simple (area-weighted) global average over space and time. On the other hand, the global-mean Stefan-Boltzmann feedback is given by $\overline{\lambda_{SB}} = -4\sigma\overline{T_e}^3$, where $\overline{T_e}$ is an effective emission temperature for the planet defined from global-mean OLR. This is neither a temperature-change-weighted mean nor a simple average of lo-

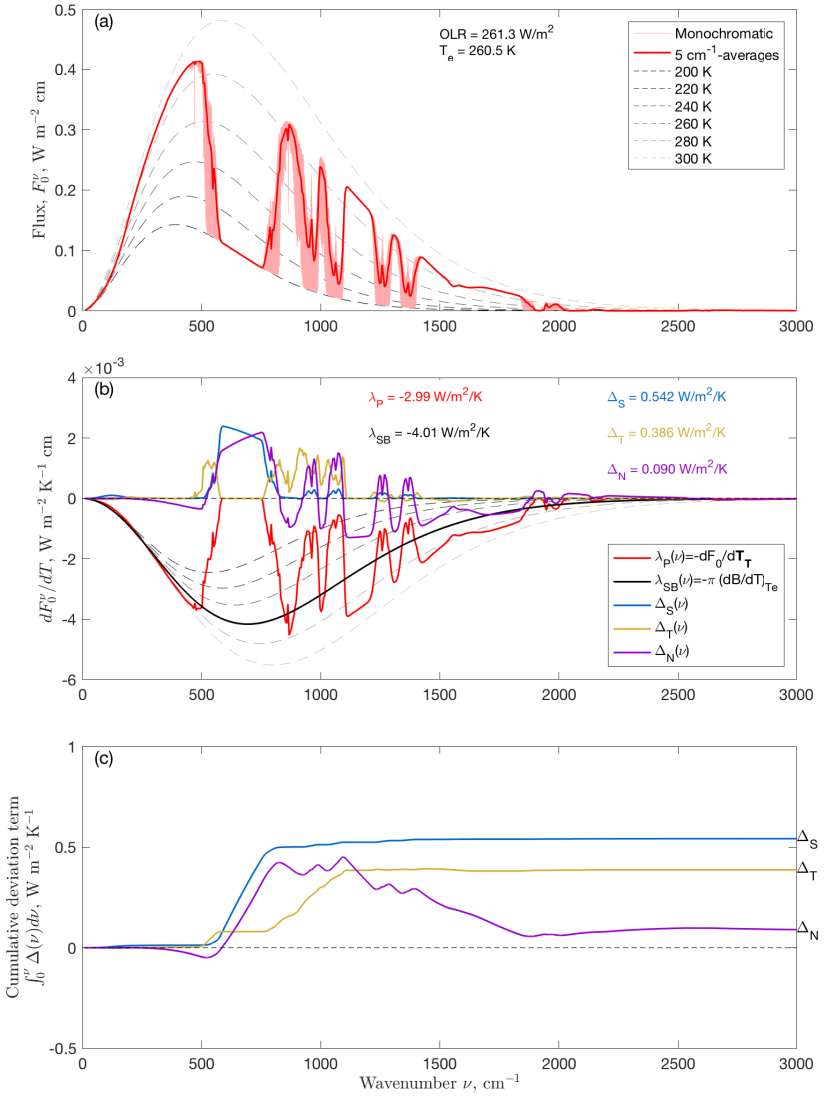

Figure 5. As in Figures 1 and 2 but for an atmosphere with no H_2O and instead 19.5% CO_2; the temperature profile follows a dry adiabat in the troposphere up to an isothermal stratosphere at 200 K. a) Outgoing infrared flux spectrum; b) Spectra of feedbacks and three deviation terms. c) Cumulative integrals from 0 to wavenumber ν of each deviation term.

cal Stefan-Boltzmann feedbacks. Fortunately, both artifacts of averaging turn out to be relatively small compared to the dominant effect of stratospheric masking.

5.1 Pattern covariance and the Planck Feedback

Most climate models show warming patterns that maximize near the north pole in winter, where the Planck feedback is also anomalously positive (least negative), so we expect the temperature-change-weighted Planck feedback to be less negative than its simple area-averaged value. We quantify this difference by using information about how the Planck feedback varies in space and time, together with projected climate model warming patterns.

We use the Soden et al. (2008) all-sky radiative kernel from the GFDL model, which has a spatial resolution of 2 degrees latitude by 2.5 degrees longitude, 17 vertical levels, and monthly temporal resolution. In order to calculate the local Planck feedback, we sum the temperature kernel from levels between the surface and tropopause (corresponding to 1K warming at each level), with tropopause pressure defined by the simple approximate expression $p_{tpp} = 300 - 200 \cos\phi$ hPa. We denote the temperature-change-weighted global-mean Planck feedback as $\overline{\lambda_P}^{(1,1,1)}$, with the superscripts following the overline indicating that covariance between warming pattern and local Planck feedback is included for latitude, longitude, and time of year. Similarly, we denote the simple area-weighted mean Planck feedback as $\overline{\lambda_P}^{(0,0,0)}$, to indicate that it includes no covariance between warming and local feedback. No warming pattern is required to calculate $\overline{\lambda_P}^{(0,0,0)}$, as it represents the simple mean of local Planck feedbacks. Using the Soden et al. (2008) kernel, and with the tropopause defined as above, we find $\overline{\lambda_P}^{(0,0,0)} = -3.263$ W m^{-2} K^{-1}.

We use output from the abrupt CO_2 quadrupling and historical scenarios of the Climate Model Intercomparison Project, phase 6, taking the temperature difference between the last 10 years of the abrupt $4\times CO_2$ simulation and the first 10 years of the historical simulation to represent the temperature change pattern. We use the mean and inter-model spread from 19 models, with models listed in Table C1. Monthly temperature change patterns are interpolated to the same horizontal grid as the radiative kernel to compute the covariance between the warming pattern and local Planck feedback. Averaging across these simulations, we find $\overline{\lambda_P}^{(1,1,1)} = -3.185$ W m^{-2} K^{-1} – about 0.08 W m^{-2} K^{-1} more positive than the simple mean $\overline{\lambda_P}^{(0,0,0)}$. This 0.08 W m^{-2} K^{-1} difference due to covariance between the warming pattern and local feedback is not negligible compared to the total 0.5 W m^{-2} K^{-1} gap between $\overline{\lambda_P}$ and $\overline{\lambda_{SB}}$, but it cannot explain the bulk of the discrepancy. In Appendix C (and Table C1, see "multi-model mean" row near the bottom), we show that this term occurs mostly due to the covariance of Planck feedback and warming patterns in latitude, with secondary effects from the combined covariance of the two quantities in latitude and time of year, and negligible effects from including covariance in longitude.

5.2 Global averaging of the Stefan-Boltzmann feedback

We now briefly address and dismiss the possibility that the Stefan-Boltzmann computed from global-mean OLR might differ appreciably from an average of local Stefan-Boltzmann feedbacks. The global-mean effective emission temperature is defined based on the global-mean OLR, $\overline{F_0}$, as $\overline{T_e} = (\overline{F_0}/\sigma)^{1/4}$. This implies that $\overline{\lambda_{SB}} = -4\sigma^{1/4}\overline{F_0}^{3/4}$. Local values of T_e, on the other hand, are defined using local outgoing fluxes F_0, so the average of local Stefan-Boltzmann feedbacks is given by $-4\sigma^{1/4}\overline{F_0^{3/4}}$. Since the 3/4 power is concave down, the Stefan-Boltzmann feedback based on global-mean OLR will always be more negative than the global-mean of local Stefan-Boltzmann feedbacks. Taking $F_0 = \overline{F_0} + F_0'$, and expanding $F_0^{3/4}$ as:

$$F_0^{3/4} = \left(\overline{F_0} + F_0'\right)^{3/4} \approx \overline{F_0}^{3/4}\left(1 + \frac{3F_0'}{4\overline{F_0}} - \frac{3(F_0')^2}{32\overline{F_0}^2} + ...\right), \tag{8}$$

gives a difference:

$$-4\sigma^{1/4}\left(\overline{F_0}^{3/4} - \overline{F_0^{3/4}}\right) \approx -4\sigma^{1/4}\overline{F_0}^{3/4}\left(\frac{3\overline{(F_0')^2}}{32\overline{F_0}^2}\right). \tag{9}$$

In words, the relative error incurred by taking the global-average of the OLR first, rather than calculating local Stefan-Boltzmann feedbacks and then averaging them, is given roughly by 3/32 times the spatiotemporal variance of OLR, divided by the square of the global-mean OLR. Using daily all-sky OLR observations from satellite (uninterpolated OLR

data provided by the NOAA/OAR/ESRL PSL, Boulder, Colorado, USA, from their website at `https://psl.noaa.gov/data/gridded/data.uninterp_OLR.html`), we calculate $\overline{F_0} = 232.1$ W m^{-2}, and $\overline{(F_0')^2} = 1659$ W^2 m^{-4}, which gives an estimated error of 0.01 W m^{-2} incurred by globally averaging OLR before calculating the Stefan-Boltzmann feedback. The binomial expansion used here also turns out to be an extremely good approximation, with values of $-4\sigma \overline{F_0}^{3/4}$ and $-4\sigma \overline{F_0}^{3/4}(1-\frac{3}{32}\overline{(F_0')^2}/\overline{F_0}^2)$ differing by less than 0.001 W m^{-2}. To recap: we consider this $\sim$0.01 W m^{-2} artifact of global averaging of the Stefan-Boltzmann feedback to be negligibly important – for Earth, its value is so small because the 3/4 power is a weakly nonlinear function, and because the variations in OLR are small relative its mean value.

6 Discussion and Conclusions

We have used single-column calculations with both a line-by-line and a correlated-k radiative transfer model to show that the deviation between local Planck and Stefan-Boltzmann feedbacks can be exactly accounted for by three deviation terms – a dominant term related to stratospheric masking, and two smaller, partly cancelling terms due to temperature-dependent opacity and nonlinear averaging. Stratospheric masking increases λ_P relative to λ_{SB} by $\sim$0.5 W m^{-2} K^{-1} near global-mean surface temperatures, with a smaller contribution at higher surface temperatures when the stratosphere is thinner and a larger contribution at lower surface temperatures when the stratosphere is thicker. Temperature-dependent opacity and nonlinear averaging each have magnitudes of about 0.1 W m^{-2} K^{-1} but opposing signs; temperature-dependent opacity acts as a positive feedback whereas nonlinear averaging acts as a negative feedback near present global-mean surface temperatures. The stratospheric masking and temperature-dependent opacity terms both depend on surface temperature, making λ_P more sensitive to local surface temperatures than λ_{SB} is, and potentially accounting for over a third of the meridional variation in the Planck feedback.

We have also used climate model patterns for warming and the Planck feedback from a radiative kernel to show that two possible artifacts of global averaging explain only a small fraction of the $\sim$0.5 W m^{-2} K^{-1} difference between global-mean Planck and Stefan-Boltzmann feedbacks (Section 5). We find the covariance of warming pattern and local Planck feedbacks causes the global-mean Planck feedback, $\overline{\lambda_P}$, to be about 0.1 W m^{-2} K^{-1} more positive than the simple areal average of local Planck feedbacks, and that nonlinearity of global averaging is insignificant for calculating the global-mean Stefan-Boltzmann feedback.

This paper has focused on clear-sky conditions; cloud cover would modify the magnitudes of some of the local deviation terms. The stratospheric masking term would be unchanged by clouds, since the stratospheric emission missing from the Planck feedback under the assumption of no stratospheric temperature change is entirely independent of (tropospheric) clouds. Low clouds are unlikely to greatly alter the picture presented in this paper, though if they were to fall above a moist boundary layer with strong H_2O continuum absorption in the Tropics, they might make the temperature-dependent opacity term more positive at high temperatures. Clouds could in some situations make Δ_N more positive by modifying the part of the nonlinear averaging term arising from averaging over heights, as discussed in Appendix B. This would be particularly likely for cold clouds of optical thickness $\sim$1, or in the case of a scene with partial cover by high thick clouds.

Our results indicate that a small possible cause of inter-model spread in the Planck feedback could arise from the water vapor continuum. A decrease in water vapor continuum absorption with temperature (holding vapor pressure fixed) is empirically well-established, and incorporated into the prevailing MT_CKD continuum model which is used by both LBLRTM and RRTMG (Mlawer et al., 2012), as well as by many other ra-

diation codes in climate models (e.g., Oreopoulos et al., 2012). Nevertheless, experimental studies disagree on how strongly continuum absorption decreases with warming (Cormier et al., 2005), and the physical mechanisms underlying the mid-infrared water vapor continuum – whether related primarily to water vapor dimers or to far wings of strong lines in rotational and rotational-vibrational bands – still remain controversial (e.g., Shine et al., 2012). Furthermore, the temperature-dependence of the water vapor self-continuum in MT_CKD has recently been updated (Mlawer et al., 2023), though it is not clear how much of an impact this might have on our results. Overall, uncertainty in water vapor continuum absorption could affect Δ_T, especially at high temperatures where the impact of the continuum region is strongest.

For Earth-like conditions, stratospheric masking is the dominant deviation term between the local Planck and Stefan-Boltzmann feedbacks. Because Δ_S depends on stratospheric optical thickness, it can also be altered by anthropogenic greenhouse gases – including effects on stratospheric H_2O from CH_4 oxidation. Using the same reference temperature profile as in Figure 2, a doubling of CO_2, stratospheric H_2O, and O_3, lead to respective increases in Δ_S by 0.05, 0.03, and 0.04 W m^{-2} K^{-1}. The historical combination of small decreases in global stratospheric O_3, together with increases in CO_2 and stratospheric H_2O (e.g., Solomon et al., 2010), has likely made the Planck feedback more positive due to increasing stratospheric opacity. Although these effects are small in the historical period, they will grow in the future and should be accounted for in feedback analysis of climate model simulations that use CO_2 concentrations many times larger than present values. Stratospheric opacity also differs appreciably between the two radiation codes that we used, raising questions about whether any systematic biases exist in stratospheric opacity in climate models. It is worth emphasizing that such variations in stratospheric opacity will have real implications for climate sensitivity because they make the Planck feedback less stabilizing: they are not simply an accounting exercise.

Some preliminary investigation suggests that the stratospheric portion of a temperature kernel for a climate model will generally give a good approximation of the stratospheric masking term. It may be biased slightly low, because it also includes a term associated with temperature-dependent opacity of the stratosphere, $\left(\frac{\delta F_0^\nu}{\delta T_S}\right)_{\text{optics}}$, which does not appear in the standard Planck feedback (we noted that it does appear in the "full-column" Planck feedback in Equation 7). In our reference atmosphere above, this additional term is a slightly negative -0.03 W m^{-2} K^{-1} because warming stratospheric CO_2 and O_3 increases their opacity and leads to a decrease in outgoing flux from the troposphere and surface. Future work could build on our findings here and try to use radiative kernels to close the gap between the Stefan-Boltzmann feedback and Planck feedback in climate model output.

At least two other possible conventions for the Planck feedback would eliminate the stratospheric masking deviation term and thus lead to a much smaller difference of the Planck feedback from the Stefan-Boltzmann estimate. First, one could easily take the "full-column" Planck feedback perspective, where the stratosphere and troposphere are both warmed uniformly. Second, one could compute a Planck feedback at the tropopause from surface and tropospheric warming. We have found that either of these alternative Planck feedbacks lies within ∼0.05 W m^{-2} K^{-1} of an appropriately defined Stefan-Boltzmann feedback. In the former case, the lack of stratospheric warming associated with surface and tropospheric warming would appear as a positive component of the lapse-rate feedback rather than as a positive component of the Planck feedback. In the latter case, the downward flux changes at the tropopause associated with stratospheric adjustment to a warmer and moister troposphere would need to be accounted for, and would appear as a positive feedback to tropospheric warming (this would be a complement to the negative top-of-atmosphere feedback considered by Wang & Huang, 2020). As noted in the introduction, these alternative choices amount to differences in accounting and do not

result in any changes in climate sensitivity relative to current conventions. They might, however, help to clarify that there is a positive feedback of ∼0.5 W m^{-2} K^{-1} implied by a stratosphere that warms little when the troposphere and surface warm.

We close by noting that stratospheric masking can be included in a simple view of the total clear-sky longwave feedback – which includes Planck, water vapor, and lapse rate components – by slightly reframing the central result of Ingram (2010). Ingram (2010), highlighting the seminal work of Simpson (1928), clarified that spectral regions where water vapor makes the atmosphere optically thick show nearly zero change in outgoing infrared flux with warming (at constant relative humidity), while all other wavenumbers will show a 'Planckian' increase in flux with warming (following $dB^{\nu}(T_b^{\nu})/dT$). More recently, Jeevanjee et al. (2021) explicitly showed that Ingram's result is naturally captured when computing climate feedbacks with relative humidity held fixed, though other studies have emphasized that the outgoing flux is not perfectly constant with surface warming in water vapor bands due to narrowing of water vapor lines and foreign broadening effects (Raghuraman et al., 2019; Feng et al., 2023). Accounting for stratospheric masking slightly revises Ingram's rule: any spectral regions that are not optically thick either to water vapor *or in the stratosphere* will to first-order show a 'Planckian' increase in flux with warming. This has a real effect on Earth's climate sensitivity relative to a hypothetical world where stratospheric opacity was much smaller. The Planck feedback is less stabilizing than the Stefan-Boltzmann feedback – and as a consequence, Earth's total climate feedback is less stabilizing overall – because the stratosphere does not warm along with the surface and troposphere. This positive feedback is implicitly embodied in the gap between λ_P and λ_{SB}, effectively hidden in all current climate model analysis that uses the conventional no-stratospheric-warming definition of the Planck feedback. The stratosphere thus deserves to be recognized as a key player in Earth's climate sensitivity, even if its contribution arises because of its thermal passivity.

Appendix A : Calculations with LBLRTM and RRTMG

We use several calculations with the standard LBLRTM code (and the RRTMG code as well), as well as with a modified code (for each model, respectively) where the temperatures seen by gas optics only are increased by 1K at all included levels, to isolate the local deviation between Planck and Stefan-Boltzmann feedbacks from each term in Equations 5 and 6:

1. A top-of-atmosphere flux control calculation gives a reference infrared flux spectrum F_0^{ν} and thus defines $T_e = (\int_0^{\infty} F_0^{\nu} d\nu/\sigma)^{1/4}$ and $\lambda_{SB} = -4\sigma T_e^3$.
2. A tropopause-flux control calculation defines an infrared flux spectrum at the tropopause, F_T^{ν} (the subscript $_T$ indicating tropopause flux).
3. A top-of-atmosphere flux, troposphere-cooled calculation uses tropospheric and surface temperatures 1 K cooler than the control calculation. The flux difference between this calculation and the control gives $\lambda_P = \delta F_0^{\nu}/\delta T_T$ following Equation 1.
4. A tropopause-flux, troposphere-cooled calculation gives an estimate of $\delta F_T^{\nu}/\delta T_T$, from which we calculate the (spectrally-resolved) stratospheric emissivity as:

$$\epsilon_S = 1 - \frac{\delta F_0^{\nu}/\delta T_T}{\delta F_T^{\nu}/\delta T_T}. \tag{A1}$$

5. A tropopause-flux, troposphere-cooled calculation using the modified code to calculate gas optical properties from the control temperature profile. Comparing this calculation with the tropopause-flux troposphere-cooled calculation (where gas optical properties also see the temperature perturbation) then allows us to calculate $(\delta F_T^{\nu}/\delta T_T)_{\text{optics}}$ directly, and $(\delta F_T^{\nu}/\delta T_T)_{\text{Planck}}$ as the difference $\delta F_T^{\nu}/\delta T_T - (\delta F_T^{\nu}/\delta T_T)_{\text{optics}}$. The top-of-atmosphere flux differences $(\delta F_0^{\nu}/\delta T_T)_{\text{Planck}}$ and $(\delta F_0^{\nu}/\delta T_T)_{\text{optics}}$ can

then be calculated by multiplying the respective tropopause flux differences by $(1-\epsilon_S)$ to account for stratospheric attenuation.

6. A top-of-atmosphere flux, full-column cooled calculation using the modified code to calculate gas optical properties from the control temperature profile. Comparing this calculation with the control case gives $(\delta F_0^\nu/\delta T_T)_{\text{Planck}}+(\delta F_0^\nu/\delta T_S)_{\text{Planck}}$, and thus allows us to isolate the change in stratospheric Planck source term by subtracting our previous calculation of $(\delta F_0^\nu/\delta T_T)_{\text{Planck}}$.

Appendix B : The nonlinear averaging terms

The nonlinear averaging deviation term calculated above, Δ_N, does not distinguish between the relative importance of nonlinearity in averaging over heights, as opposed to averaging over wavenumbers. Following logic similar to that in section 5.2, an approximate power-law form of the monochromatic flux can be used to understand why the effect of nonlinear averaging over heights is generally small, and thus why Δ_N is mostly determined by nonlinear averaging across wavenumbers. The Planck function,

$$B^\nu(T) = \frac{2\pi h c^2 \nu^3}{\exp\left(\frac{hc\nu}{kT}\right) - 1}, \tag{B1}$$

which describes the radiance of a blackbody at temperature T (where h is Planck's constant, c is the speed of light, and k is Boltzmann's constant), can be approximated near a reference temperature T_0 by:

$$B^\nu(T) = B^\nu(T_0)\left(\frac{T}{T_0}\right)^\alpha \tag{B2}$$

$$\alpha \equiv \frac{d\log B^\nu(T_0)}{d\log T} = \frac{hc\nu}{kT_0}\frac{\exp\left(\frac{hc\nu}{kT_0}\right)}{\exp\left(\frac{hc\nu}{kT_0}\right)-1}. \tag{B3}$$

(e.g., Jeevanjee & Fueglistaler, 2020). This exponent, α, approaches 1 for photons with much less than average thermal energies ($hc\nu/(kT_0) << 1$), and asymptotes from above to $hc\nu/(kT_0)$ for photons with much greater than average thermal energies ($hc\nu/(kT_0) >> 1$). Denoting the arithmetic mean of emitting temperatures at a single wavenumber as $\overline{T}$, and departures from this emitting temperature as T', it can be shown that:

$$\frac{\overline{dF}}{dT} = \left[\frac{\alpha\pi B^\nu(T_0)}{T_0^\alpha}\right]\overline{T^{\alpha-1}} \approx \left[\frac{\alpha\pi B^\nu(T_0)}{T_0}\right]\overline{T}^{\alpha-1}\left(1+\frac{(\alpha-1)(\alpha-2)}{2}\frac{\overline{(T')^2}}{\overline{T}^2}\right) \tag{B4}$$

$$\left(\frac{dF}{dT}\right)_{T(\overline{F})} = \left[\frac{\alpha\pi B^\nu(T_0)}{T_0^\alpha}\right]\left(\overline{T^\alpha}\right)^{1-\frac{1}{\alpha}} \approx \left[\frac{\alpha\pi B^\nu(T_0)}{T_0}\right]\overline{T}^{\alpha-1}\left(1+\frac{(\alpha-1)^2}{2}\frac{\overline{(T')^2}}{\overline{T}^2}\right) \tag{B5}$$

where the latter approximation of each expression has used a Taylor expansion and retained only the variance of emitting temperatures but not higher-order terms, by assuming that $T'/\overline{T}$ is small. Even before each approximation, it should be clear that $\overline{dF}/dT < (dF/dT)_{T(\overline{F})}$, because $\alpha > 1$ and thus $(dF/dT)_{T(\overline{F})}$ is a concave function of the flux derivatives involved in $\overline{dF}/dT$ (e.g., with $\alpha = 4$, $(dF/dT)_{T(\overline{F})}$ is the 3/4 power of an average of the 4/3 power of the flux derivatives used to calculate $\overline{dF}/dT$). Using these approximate forms, the difference between the two terms is given by:

$$\left(\frac{dF}{dT}\right)_{T(\overline{F})} - \frac{\overline{dF}}{dT} \approx \left[\frac{\alpha\pi B^\nu(T_0)}{T_0}\right]\overline{T}^{\alpha-1}\left[\frac{\alpha-1}{2}\frac{\overline{(T')^2}}{\overline{T}^2}\right]. \tag{B6}$$

In a relative sense, this difference is very close to $\frac{\alpha-1}{2}(\overline{(T')^2}/\overline{T}^2)$, and thus depends on the variance of the emitting temperatures relative to the square of the mean emitting temperature. Note that the result from section 5.2 is a specific example of this difference that can be recovered by using $\alpha = 4$ and $(\overline{(F')^2}/\overline{F}^2) = 16(\overline{(T')^2}/\overline{T}^2)$. We can

roughly estimate a typical relative deviation from the mean emitting temperature based on how rapidly the logarithm of atmospheric temperature changes with the logarithm of monochromatic optical thickness (using the reasoning that emission mostly occurs within one factor of e near $\tau = 1$). Using the chain rule to express $d\log T/d\log\tau$ gives:

$$\frac{|T'|}{\overline{T}} \approx \frac{d\log T}{d\log\tau} = \frac{d\log T}{d\log p} \times \frac{d\log p}{d\log\tau} \approx \frac{R\Gamma}{g}\frac{1}{\beta}, \tag{B7}$$

where Γ is the lapse rate, and use of $\beta = d\log\tau/d\log p$ follows Jeevanjee and Fueglistaler (2020). Applying this expression for a few examples shows why the deviation of $(dF/dT)_{T(\overline{F})}$ from $\overline{dF}/dT$ is typically small. For a well-mixed gas such as CO_2, $\beta = 2$ due to pressure broadening; if emission is mostly tropospheric, we can take $\Gamma \approx 6.5$ K km^{-1} to obtain $|T'|/\overline{T} \approx 0.1$, and thus a nonlinear averaging deviation on the order of 1-2% from averaging across heights. For wavenumbers where CO_2 emits from the stratosphere, however, the magnitude of the lapse rate is greatly reduced and thus the deviation is smaller by about a factor of 10. For H_2O emitting from the troposphere, the larger value of $\beta \approx 5$ due to decay in H_2O concentration with height leads to expected deviations on the order of 0.1% (and made further smaller by the low values of α in the H_2O rotational band). Note that the key parameter for the relative magnitude of this deviation term, $\frac{\alpha-1}{2}(\overline{(T')^2}/\overline{T}^2)$, can also be written as $\frac{\alpha-1}{2\alpha^2}\gamma^2$, where $\gamma = d\log B/d\log\tau$ is the key parameter governing the validity of the cooling-to-space approximation (valid for $\gamma << 1$), derived by Jeevanjee and Fueglistaler (2020). The connection between neglect of the within-wavenumber nonlinear averaging term and the validity of the cooling-to-space approximation arises because both conditions hold best when the levels that emit to space have only a small variation in temperature (leading to small variations in the Planck source function).

One plausible situation where nonlinear averaging across heights could be more important would be the case of a high cloud of optical thickness ∼1 near the tropopause, in a spectral region with very low clear-sky optical thickness and a large value of α: in such conditions averaging across heights might introduce a deviation as large as 10% of the actual monochromatic flux change. This caveat noted, we conclude that nonlinear averaging across heights is generally a small deviation term relative to the portion of Δ_N associated with nonlinear averaging across wavenumbers.

Appendix C : Decomposing sources of pattern covariance

To identify the sources of pattern covariance between warming and local Planck feedbacks, we can compute global-average feedbacks that include the structure of both quantities across some subset of the three dimensions (latitude, longitude, time) but not others. We first define the local warming ratio $r(y,\theta,t) = \Delta T(y,\theta,t)/\overline{\Delta T}^{(y,\theta,t)}$ as the ratio of local temperature change $\Delta T(y,\theta,t)$ – dependent on the sine of latitude ($y = \sin\phi$), the longitude θ, and the month of year t – to the global and annual-mean warming $\overline{\Delta T}^{(y,\theta,t)}$. Parentheses following the overline symbol here indicate the dimensions over which the average is taken; e.g., $\overline{\Delta T}^{(\theta)}$ would be the average of the temperature change over longitude, retaining dependence on latitude and time of year. Taking all combinations gives eight different global-average Planck feedbacks which either include or neglect covariance between the warming pattern and the Planck feedback over each of the three dimensions:

$$\begin{aligned}
\overline{\lambda_P}^{(1,1,1)} &= \overline{\lambda_P r}^{(y,\theta,t)} \\
\overline{\lambda_P}^{(1,1,0)} &= \overline{\overline{\lambda_P}^{(t)}\overline{r}^{(t)}}^{(y,\theta)} \\
\overline{\lambda_P}^{(1,0,1)} &= \overline{\overline{\lambda_P}^{(\theta)}\overline{r}^{(\theta)}}^{(y,t)} \\
\overline{\lambda_P}^{(0,1,1)} &= \overline{\overline{\lambda_P}^{(y)}\overline{r}^{(y)}}^{(\theta,t)} \\
\overline{\lambda_P}^{(1,0,0)} &= \overline{\overline{\lambda_P}^{(\theta,t)}\overline{r}^{(\theta,t)}}^{(y)}
\end{aligned}$$

$$\begin{aligned}
\overline{\lambda_P}^{(0,1,0)} &= \overline{\overline{\lambda_P}^{(y,t)}\overline{r}^{(y,t)}}^{(\theta)} \\
\overline{\lambda_P}^{(0,0,1)} &= \overline{\overline{\lambda_P}^{(y,\theta)}\overline{r}^{(y,\theta)}}^{(t)} \\
\overline{\lambda_P}^{(0,0,0)} &= \overline{\lambda_P}^{(y,\theta,t)}\overline{r}^{(y,\theta,t)}. \qquad \text{(C1)}
\end{aligned}$$

Note here that $\overline{\lambda_P}^{(0,0,0)}$ is the simple average previously defined, and $\overline{\lambda_P}^{(1,1,1)}$ is the full temperature-change-weighted average including covariance of Planck feedback and warming over latitude, longitude, and time of year. Subtracting $\overline{\lambda_P}^{(0,0,0)}$ from each gives a pattern covariance deviation $\Delta_C^{(\cdot,\cdot,\cdot)} = \overline{\lambda_P}^{(\cdot,\cdot,\cdot)} - \overline{\lambda_P}^{(0,0,0)}$, with values for each term in each model shown in Table C1. Comparing the calculated values in Table C1 shows that latitudinal structure dominates the covariance of the warming pattern and local Planck feedback. Temporal structure matters as well, but only when included together with latitudinal structure, and longitudinal structure is almost entirely negligible for the pattern covariance of warming and Planck feedback. To first order, one can think of the pattern covariance deviation term as arising because warming and Planck feedbacks are larger at the poles than in the tropics, and to second order because both are also larger at the poles in (local) winter than in summer.

Open Research Section

Model output and scripts used to make figures in this paper are available in a Zenodo repository: `https://doi.org/10.5281/zenodo.8071220` (Cronin & Dutta, 2023).

Acknowledgments

Work on this paper was supported by NSF Atmospheric Chemistry grant AGS-1906719: "Advancing the Understanding of the Impacts of Wave-Induced Temperature Fluctuations on Atmospheric Chemistry". We thank Susan Solomon, Peter Molnar, Nick Lutsko, Daniel Koll, and Aaron Donohoe for helpful comments on early drafts of this manuscript, Nadir Jeevanjee, Shiv Priyam Raghuraman and several anonymous reviewers for useful feedback on multiple versions of the paper in the review process (particular thanks is due to a reviewer who penned two lengthy and rigorous reviews that heavily reshaped the paper and led to the coinage of "Stefan-Boltzmann feedback"), and AER for freely providing LBLRTM (available at `http://rtweb.aer.com/lblrtm.html`). We acknowledge the World Climate Research Programme's Working Group on Coupled Modelling, which is responsible for CMIP, and we thank the climate modeling groups (listed in Table C1 of this paper) for producing and making available their model output.

References

Bader, D. C., Leung, R., Taylor, M., & McCoy, R. B. (2019). E3SM-Project E3SM1.0 model output prepared for CMIP6; historical, abrupt-4xCO2. *Earth System Grid Federation*. doi: 10.22033/ESGF/CMIP6.4491

Bethke, I., Wang, Y., Counillon, F., Kimmritz, M., Fransner, F., Samuelsen, A., ... Keenlyside, N. (2019). NCC NorCPM1 model output prepared for CMIP6; historical, abrupt-4xCO2. *Earth System Grid Federation*. doi: 10.22033/ESGF/CMIP6.10862

Bony, S., Colman, R., Kattsov, V. M., Allan, R. P., Bretherton, C. S., Dufresne, J.-L., ... Webb, M. J. (2006). How well do we understand and evaluate climate change feedback processes? *Journal of Climate*, *19*(15), 3445–3482. doi: 10.1175/JCLI3819.1

Boucher, O., Denvil, S., Levavasseur, G., Cozic, A., Caubel, A., Foujols, M.-A., ... Marchand, M. (2021). IPSL IPSL-CM6A-LR-INCA model output prepared for CMIP6; historical, abrupt-4xCO2. *Earth System Grid Federation*. doi: 10.22033/ESGF/CMIP6.13584

Table C1. CMIP6 models used and decomposition of meridional covariance deviation for each, with notation following Equation C1.

Climate Model	Citation	$\Delta_C^{(1,1,1)}$ W m^{-2} K^{-1}	$\Delta_C^{(1,1,0)}$	$\Delta_C^{(1,0,1)}$	$\Delta_C^{(0,1,1)}$	$\Delta_C^{(1,0,0)}$	$\Delta_C^{(0,1,0)}$	$\Delta_C^{(0,0,1)}$
ACCESS-CM2	Dix et al. (2019)	0.071	0.063	0.080	-0.002	0.072	-0.002	0.001
BCC-CSM2-MR	Wu et al. (2018)	0.088	0.073	0.098	0.000	0.083	-0.001	0.002
BCC-ESM1	Zhang et al. (2019)	0.093	0.080	0.102	0.001	0.088	0.000	0.002
CanESM5	Swart et al. (2019)	0.081	0.069	0.086	0.002	0.074	0.001	0.001
CESM2	Danabasoglu (2019)	0.074	0.062	0.086	-0.001	0.075	-0.001	0.001
E3SM1.0	Bader et al. (2019)	0.080	0.074	0.088	-0.001	0.082	-0.001	0.001
FGOALS-f3-L	Yu (2019)	0.103	0.085	0.113	0.000	0.094	-0.002	0.002
GFDL-CM4	Guo et al. (2018)	0.072	0.065	0.081	-0.002	0.074	-0.002	0.000
GISS-E2.1G	NASA/GISS (2018)	0.052	0.042	0.058	-0.001	0.048	0.000	0.001
GISS-E2.1H	NASA/GISS (2019)	0.080	0.067	0.093	-0.004	0.080	-0.005	0.001
IPSL-CM6A-LR-INCA	Boucher et al. (2021)	0.072	0.066	0.078	0.000	0.072	0.001	0.001
KACE1.0-G	Byun et al. (2019)	0.072	0.062	0.080	-0.001	0.071	-0.001	0.001
KIOST-ESM	Kim et al. (2019)	0.042	0.029	0.049	-0.001	0.037	-0.002	0.001
MCM-UA-1-0	Stouffer (2019)	0.084	0.068	0.093	-0.001	0.078	0.000	0.000
MIROC6	Tatebe and Watanabe (2018)	0.049	0.039	0.059	0.001	0.049	0.000	0.002
MIROC-ES2L	Hajima et al. (2019)	0.054	0.043	0.060	0.000	0.049	-0.001	0.001
MRI-ESM2.0	Yukimoto et al. (2019)	0.099	0.084	0.107	-0.002	0.093	-0.002	0.000
NESMv3	Cao and Wang (2019)	0.095	0.085	0.099	0.001	0.090	0.000	0.001
NorCPM1	Bethke et al. (2019)	0.124	0.111	0.128	0.001	0.115	0.001	0.001
Multi-model mean		0.078	0.067	0.086	-0.001	0.075	-0.001	0.001
Multi-model std. dev.		0.020	0.019	0.020	0.001	0.018	0.001	0.001

Byun, Y.-H., Lim, Y.-J., Sung, H. M., Kim, J., Sun, M., & Kim, B.-H. (2019). NIMS-KMA KACE1.0-G model output prepared for CMIP6; historical, abrupt-4xCO2. *Earth System Grid Federation*. doi: 10.22033/ESGF/CMIP6.8348

Cao, J., & Wang, B. (2019). NUIST NESMv3 model output prepared for CMIP6; historical, abrupt-4xCO2. *Earth System Grid Federation*. doi: 10.22033/ESGF/CMIP6.8719

Clough, S. A., Shephard, M. W., Mlawer, E. J., Delamere, J. S., Iacono, M. J., Cady-Pereira, K., ... Brown, P. D. (2005). Atmospheric radiative transfer modeling: A summary of the AER codes. *J. Quant. Spectrosc. Radiat. Transfer*, *91*, 233-244.

Cormier, J. G., Hodges, J. T., & Drummond, J. R. (2005). Infrared water vapor continuum absorption at atmospheric temperatures. *The Journal of Chemical Physics*, *122*(114309). doi: 10.1063/1.1862623

Cronin, T., & Dutta, I. (2023, June). *Figure scripts and output files from "How well do we understand the Planck feedback?"*. Zenodo. Retrieved from `https://doi.org/10.5281/zenodo.8071220` doi: 10.5281/zenodo.8071220

Danabasoglu, G. (2019). NCAR CESM2-WACCM model output prepared for CMIP6; historical, abrupt-4xCO2. *Earth System Grid Federation*. doi: 10.22033/ESGF/CMIP6.10039

Dix, M., Bi, D., Dobrohotoff, P., Fiedler, R., Harman, R., Ian Law, Mackallah, C., ... Yang, R. (2019). CSIRO-ARCCSS ACCESS-CM2 model output prepared for CMIP6; historical, abrupt-4xCO2. *Earth System Grid Federation*. doi: 10.22033/ESGF/CMIP6.4237

Elsasser, W. (1942). *Heat transfer by infrared radiation in the atmosphere.* Blue Hill Meteorological Observatory.

Feldl, N., & Roe, G. H. (2013). The nonlinear and nonlocal nature of climate feedbacks. *Journal of Climate*, *26*, 8289–8304. doi: 10.1175/JCLI-D-12-00631.1

Feng, J., Paynter, D., & Menzel, R. (2023). How a Stable Greenhouse Effect on Earth Is Maintained Under Global Warming. *Journal of Geophysical Research: Atmospheres*, *128*. doi: 10.1029/2022JD038124

Fu, Q., & Liou, K. N. (1992). On the correlated k-distribution method for radiative transfer in nonhomogeneous atmospheres. *Journal of the Atmospheric Sciences*, *49*(22), 2139–2156.

Guo, H., John, J. G., Blanton, C., McHugh, C., Nikonov, S., Radhakrishnan, A., ... Zhang, R. (2018). NOAA-GFDL GFDL-CM4 model output prepared for CMIP6; historical, abrupt-4xCO2. *Earth System Grid Federation*. doi: 10.22033/ESGF/CMIP6.8486

Hajima, T., Abe, M., Arakawa, O., Suzuki, T., Komuro, Y., Ogura, T., ... Tachiiri, K. (2019). MIROC MIROC-ES2L model output prepared for CMIP6; historical, abrupt-4xCO2. *Earth System Grid Federation*. doi: 10.22033/ESGF/CMIP6.5410

Hansen, J., Lacis, A., Rind, D., Russell, G., Stone, P., Fung, I., ... Lerner, J. (1984, January). Climate sensitivity: Analysis of feedback mechanisms. *Washington DC American Geophysical Union Geophysical Monograph Series*, *29*, 130–163. doi: 10.1029/GM029p0130

Hansen, J., Sato, M., & Ruedy, R. (1997). Radiative forcing and climate response. *Journal of Geophysical Research*, *102*(D6), 6831–6864.

Huang, Y., & Ramaswamy, V. (2007). Effect of the temperature dependence of gas absorption in climate feedback. *Journal of Geophysical Research: Atmospheres*, *112*(D07101). doi: 10.1029/2006JD007398

Huang, Y., Zhang, M., Xia, Y., Hu, Y., & Son, S.-W. (2016). Is there a stratospheric radiative feedback in global warming simulations? *Climate Dynamics*, *46*, 177–186. doi: 10.1007/s00382-015-2577-2

Ingram, W. (2010). A very simple model for the water vapour feedback on climate

change. *Quarterly Journal of the Royal Meteorological Society*, *136*, 30–40. doi: 10.1002/qj.546

Jeevanjee, N., & Fueglistaler, S. (2020). On the cooling to space approximation. *Journal of the Atmospheric Sciences*, *77*, 465–478. doi: 10.1175/JAS-D-18-0352.1

Jeevanjee, N., Koll, D. D. B., & Lutsko, N. (2021). "Simpson's Law" and the spectral cancellation of climate feedbacks. *Geophysical Research Letters*, *48*. doi: 10.1029/2021GL093699

Kim, Y. H., Noh, Y., Kim, D., Lee, M.-I., Lee, H. J., Kim, S. Y., & Kim, D. (2019). KIOST KIOST-ESM model output prepared for CMIP6; historical, abrupt-4xCO2. *Earth System Grid Federation*. doi: 10.22033/ESGF/CMIP6.5288

Kluft, L., Dacie, S., Brath, M., Buehler, S., & Stevens, B. (2021). Temperature-Dependence of the Clear-Sky Feedback in Radiative-Convective Equilibrium. *Geophysical Research Letters*, *48*. doi: 10.1029/2021GL094649

Loeb, N. G., Doelling, D. R., Wang, H., Su, W., Nguyen, C., Corbett, J. G., ... Kato, S. (2018). Clouds and the earth's radiant energy system (ceres) energy balanced and filled (ebaf) top-of-atmosphere (toa) edition-4.0 data product. *Journal of Climate*, *31*(2), 895–918. doi: 10.1175/JCLI-D-17-0208.1

Mlawer, E., Cady-Pereira, K., Mascio, J., & Gordon, I. (2023). The inclusion of the MT_CKD water vapor continuum model in the HITRAN molecular spectroscopic database. *Journal of Quantitative Spectroscopy and Radiative Transfer*, *306*. doi: 10.1016/j.jqsrt.2023.108645

Mlawer, E., Payne, V., Moncet, J.-L., Delamere, J., Alvarado, M., & Tobin, D. (2012). Development and recent evaluation of the MT_CKD model of continuum absorption. *Philosophical Transactions of the Royal Society A*, *370*, 2520–2556. doi: 10.1098/rsta.2011.0295

NASA/GISS. (2018). NASA-GISS GISS-E2.1G model output prepared for CMIP6; historical, abrupt-4xCO2. *Earth System Grid Federation*. doi: 10.22033/ESGF/CMIP6.6976

NASA/GISS. (2019). NASA-GISS GISS-E2.1H model output prepared for CMIP6; historical, abrupt-4xCO2. *Earth System Grid Federation*. doi: 10.22033/ESGF/CMIP6.6977

Oman, L., Waugh, D. W., Pawson, S., Stolarski, R. S., & Nielsen, J. E. (2008). Understanding the changes of stratospheric water vapor in coupled chemistry-climate model simulations. *Journal of the Atmospheric Sciences*, *65*, 3278–3291.

Oreopoulos, L., Mlawer, E., Delamere, J., Shippert, T., Cole, J., Fomin, B., ... Rossow, W. B. (2012). The continual intercomparison of radiation codes: Results from phase I. *Journal of Geophysical Research: Atmospheres*, *117*(D6). doi: https://doi.org/10.1029/2011JD016821

Raghuraman, S. P., Paynter, D., & Ramaswamy, V. (2019). Quantifying the Drivers of the Clear Sky Greenhouse Effect, 2000?2016. *Journal of Geophysical Research: Atmospheres*, *124*, 11354–11371. doi: 10.1029/2019JD031017

Shine, K. P., Ptashnik, I. V., & Radel, G. (2012). The water vapor continuum: brief history and recent developments. *Surveys in Geophysics*, *33*, 535–555. doi: 10.1007/s10712-011-9170-y

Simpson, G. C. (1928). Some studies in terrestrial radiation. *Memoirs of the Royal Meteorological Society*, *2*, 69–95.

Soden, B. J., & Held, I. M. (2006). An assessment of climate feedbacks in coupled ocean-atmosphere models. *Journal of Climate*, *19*(14), 3354-3360.

Soden, B. J., Held, I. M., Colman, R., Shell, K. M., Kiehl, J. T., & Shields, C. A. (2008). Quantifying climate feedbacks using radiative kernels. *Journal of Climate*, *21*, 3504–3520. doi: 10.1175/2007JCLI2110.1

Solomon, S., Rosenlof, K. H., Portmann, R. W., Daniel, J. S., Davis, S. M., Sanford, T. J., & Plattner, G.-K. (2010). Contributions of stratospheric water vapor to

decadal changes in the rate of global warming. *Science*, *327*, 1219–1223. doi: 10.1126/science.1182488

Stouffer, R. (2019). UA MCM-UA-1-0 model output prepared for CMIP6; historical, abrupt-4xCO2. *Earth System Grid Federation*. doi: 10.22033/ESGF/CMIP6.8882

Swart, N. C., Cole, J. N., Kharin, V. V., Lazare, M., Scinocca, J. F., Gillett, N. P., ... Sigmond, M. (2019). CCCma CanESM5 model output prepared for CMIP6; historical, abrupt-4xCO2. *Earth System Grid Federation*. doi: 10.22033/ESGF/CMIP6.3532

Tatebe, H., & Watanabe, M. (2018). MIROC MIROC6 model output prepared for CMIP6; historical, abrupt-4xCO2. *Earth System Grid Federation*. doi: 10.22033/ESGF/CMIP6.5411

Wang, Y., & Huang, Y. (2020). Stratospheric radiative feedback limited by the tropospheric influence in global warming. *Climate Dynamics*, *55*, 2343–2350. doi: 10.1007/s00382-020-05390-4

Wing, A. A., Reed, K. A., Satoh, M., Stevens, B., Bony, S., & Ohno, T. (2018). Radiative-convective equilibrium model intercomparison project. *Geoscientific Model Development*, *11*, 793–813. doi: 10.5194/gmd-11-793-2018

Wu, T., Chu, M., Dong, M., Fang, Y., Jie, W., Li, J., ... Zhang, Y. (2018). BCC BCC-CSM2MR model output prepared for CMIP6; historical, abrupt-4xCO2. *Earth System Grid Federation*. doi: 10.22033/ESGF/CMIP6.2845

Yu, Y. (2019). CAS FGOALS-f3-L model output prepared for CMIP6; historical, abrupt-4xCO2. *Earth System Grid Federation*. doi: 10.22033/ESGF/CMIP6.3176

Yukimoto, S., Koshiro, T., Kawai, H., Oshima, N., Yoshida, K., Urakawa, S., ... Adachi, Y. (2019). MRI MRI-ESM2.0 model output prepared for CMIP6; historical, abrupt-4xCO2. *Earth System Grid Federation*. doi: 10.22033/ESGF/CMIP6.6755

Zelinka, M. D., Meyers, T. A., McCoy, D. T., Po-Chedley, S., Caldwell, P. M., Ceppi, P., ... Taylor, K. E. (2020). Causes of higher climate sensitivity in CMIP6 models. *Geophysical Research Letters*, *47*. doi: 10.1029/2019GL085782

Zhang, J., Wu, T., Shi, X., Zhang, F., Li, J., Chu, M., ... Wei, M. (2019). BCC BCC-ESM1 model output prepared for CMIP6; historical, abrupt-4xCO2. *Earth System Grid Federation*. doi: 10.22033/ESGF/CMIP6.2846